Sensorless Control of Permanent-Magnet Linear Synchronous Motor Based on Modified Linear Extended State Observer

Sensorless Control of Permanent-Magnet Linear Synchronous Motor Based on Modified Linear Extended State Observer

Yue Qu
School of Engineering
Griffith University
Brisbane, Australia
siachu@163.com

Junwei Lu
School of Engineering
Griffith University
Brisbane, Australia
j.lu@griffith.edu.au

Hui Li
College of Automation Engineering
Shanghai University of Electric Power
Shanghai, China
lihui@shiep.edu.cn

Xitong Niu
KUKA Robotics China Co., Ltd
Shanghai, China
niu_xi_tong@126.com

***Abstract*—Permanent-Magnet Linear Synchronous Motor (PMLSM) transforms electric energy into linear mechanical kinetic energy without transmission mechanism which is widely used in rail transmit due to its merits of high efficiency, relatively low losses and simple mechanism. In the field oriented control of the linear motor, high-precision speed and position information are required. However, the installation of the linear grating increases the cost and complexity of the system, reduces anti-disturbance ability for mechanical structures, which may directly affect the control performance. In this paper, based on the sensorless control method, a modified linear extended state observer (MLESO) is proposed and utilized to estimate the back electromotive force. Then, the linear active rejection disturbance control (LADRC) is used to estimate and compensate system dynamics and disturbances to enhance disturbance rejection and stability of the PMLSM system. Moreover, the feedforward controller (FFC) is introduced to improve the response speed of the PMLSM. The simulation results certify that the proposed strategy has the superiority to the conventional sensorless control method.**

Keywords—PMLSM, LESO, LADRC, sensorless control, feedback controller

I. INTRODUCTION

Permanent-Magnet Linear Synchronous Motor (PMLSM) is a direct-drive motor that converts from rotational torque to linear force without any mechanical transmission[1]. In recent years, linear motors have been widely used in the fields of automated production, civil aviation transportation, military, and others due to its remarkable advantages[2]:

(1) Linear motor directly produces linear motion, the mover is generally directly connected with the loads, improving the transmission efficiency;

(2) The structure of the motion system is simple, which improves the reliability of the system and reduces the noise interference caused by mechanical friction;

(3) Linear motor has high acceleration, which can produce high linear speed in short stroke;

(4) The linear motor is not bound by centrifugal force, so the linear speed is unlimited.

In order to achieve high-precision speed and position control, field-oriented control or direct thrust control strategy is usually used in AC speed control systems [3]. However, no matter what control strategy, it requires high-precision motor speed and position information, which is usually obtained by a photoelectric encoder, tachogenerator, resolver and other sensors.

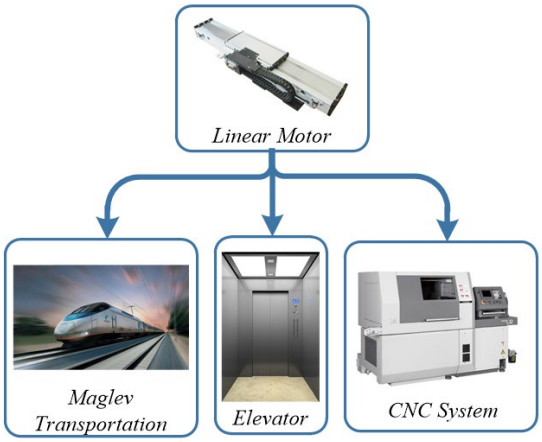

Fig. 1. Application of linear motor

And in the detection process, it will bring a series of problems to the system. Firstly, the installation of these sensors increases the cost and complexity of the system. Secondly, the installation requirements of speed and position sensors are quite high, like the flatness of installation surface[4]. Aiming at the situation that the mechanical position sensors and speed sensors are not suitable in some specific applications, researchers proposed a variety of sensorless position estimation methods in recent years. These methods calculate the PM position and speed by electromagnetic signal rather than position sensors[5,6], which commonly can be classified into two categories. One sensorless position measurement is based on the change of inductance. The armature inductance of linear motor changes periodically with the relative position of primary and secondary, which also leads to the change of armature current. Hence, the position can be expressed as a function of the rate of armature current change[7]. However, this method is suitable for the motor with a certain saliency rate. The more obvious the inductance difference between d axis and q axis is, the more accurate the position estimation is. The other sensorless method is based on back electromotive force (EMF), which can extract the position information according to the variation of amplitude and phase of back EMF. Yet this method generally shows good performance at the medium and high-speed situation, because back EMF is zero when the motor is stationary, and

978-1-7281-7210-1/21/$31.00 ©2021 IEEE

the back EMF signal is easy to be disturbed at low speed. Therefore, when the motor is accelerated to a relatively high speed by a speed open-loop control, the estimated speed, and position values can be used for the speed closed-loop control[8-18].

There are various back EMF based methods such as model reference adaptive method, extended Kalman filter and state observer method. The state observer method has been used in sensorless drive systems in recent years. In the tracking of state parameters, noise is inevitable. High-frequency noise can be removed, and low-frequency noise is retained because state observer has a similar transfer function and ability as a low pass filter. But low-frequency noise is difficult to be avoided in practice, as the offsets when the DC source voltage and phase current are measured[1]. The low-frequency noise decreases the precision and other control performance, which may be serious enough to destroy the sensorless control under a small power case.

In order to improve the control performance of PMLSM in precision and response speed, this paper proposes a modified linear extended state observer (MLESO) to remove the offsets. Meanwhile, the proposed method introduces a composite controller of linear active rejection disturbance control (LADRC) and the feedforward controller (FFC) to enhance the disturbance rejection and response speed of the PMLSM, which also ensures the PMLSM operating stably and reliably.

This paper includes six sections as follows. Section I is the introduction. In section II, the mathematical model of a linear synchronous motor in the *dq* synchronous reference frame is established. Section III proposes the novel MLESO and analyses its stability in the frequency domain. In section IV, the composite control strategy based on the sensorless control system of PMLSM is proposed. Section V illustrates the simulation results and verifies the effectiveness of the proposed control strategy. Finally, conclusions and discussion are given in section VI.

II. State Space Model of PMLSM

In the *dq* synchronous reference frame, the voltage formula and flux linkage formula of PMLSM are respectively expressed as:

$$\begin{bmatrix} u_d \\ u_q \end{bmatrix} = R_s \begin{bmatrix} i_d \\ i_q \end{bmatrix} + \frac{d}{dt}\begin{bmatrix} \lambda_d \\ \lambda_q \end{bmatrix} + \frac{\pi v}{\tau}\begin{bmatrix} -\lambda_q \\ \lambda_d \end{bmatrix}, \tag{1}$$

$$\begin{bmatrix} \lambda_d \\ \lambda_q \end{bmatrix} = \begin{bmatrix} L_d & 0 \\ 0 & L_q \end{bmatrix}\begin{bmatrix} i_d \\ i_q \end{bmatrix} + \begin{bmatrix} \lambda_{PM} \\ 0 \end{bmatrix}. \tag{2}$$

Where , u_q and i_d , i_q are voltages and currents of primary armature winding respectively, λ_d and λ_q are flux linkage of primary armature winding, λ_{PM} is the flux linkage produced by the permanent magnet. L_d and L_q are inductances, R_s is primary armature resistance, τ is pole pitch of PMLSM, v is mechanical speed.

The discontinuity between the primary core and the winding leads to the unequal mutual inductance between the three-phase windings. This means that when you transform the model to the *dq* synchronous reference frame, mutual inductance M_{dq} is not zero. But the M_{dq} is commonly small, which can be ignored in the control. Combining formula (1) and (2):

$$\begin{bmatrix} u_d \\ u_q \end{bmatrix} = R_s \begin{bmatrix} i_d \\ i_q \end{bmatrix} + A\frac{d}{dt}\begin{bmatrix} i_d \\ i_q \end{bmatrix} + \frac{\pi v}{\tau}\left\{ B\begin{bmatrix} i_d \\ i_q \end{bmatrix} + \begin{bmatrix} 0 \\ \lambda_{PM} \end{bmatrix}\right\}, \tag{3}$$

where

$$A=\begin{bmatrix} L_d & 0 \\ 0 & L_q \end{bmatrix},\ B=\begin{bmatrix} 0 & -L_q \\ L_d & 0 \end{bmatrix}.$$

Electromagnetic thrust equation can be expressed as:

$$F_{em} = \frac{3\pi n_p}{2\tau}\left[(L_d - L_q) i_d i_q + \lambda_{PM} i_q \right], \tag{4}$$

where F_{em} is electromagnetic thrust force and n_p is the number of motor pole pairs.

The mechanical motion equation of PMLSM can be written as:

$$F_{em} - F_l - Dv = (m + m_0)\frac{dv}{dt}, \tag{5}$$

where F_l is load force, D is coefficient of viscous friction, m and m_0 are moving part weight of PMLSM and load weight respectively. The model (4) also can be expressed in the α-β stationary reference frame:

$$\begin{bmatrix} u_\alpha \\ u_\beta \end{bmatrix} = R_s \begin{bmatrix} i_\alpha \\ i_\beta \end{bmatrix} + \begin{bmatrix} L_\alpha & 0 \\ 0 & L_\beta \end{bmatrix}\frac{d}{dt}\begin{bmatrix} i_\alpha \\ i_\beta \end{bmatrix} + \begin{bmatrix} e_\alpha \\ e_\beta \end{bmatrix}, \tag{6}$$

where $u_{\alpha,\beta}$, $i_{\alpha,\beta}$, $L_{\alpha,\beta}$ are the voltage, current and resistance in the stationary reference frame respectively. In addition, $e_{\alpha,\beta}$ is back EMF, which can be expressed as:

$$\begin{bmatrix} e_\alpha \\ e_\beta \end{bmatrix} = \frac{n_p \lambda_{PM} \pi}{\tau} v \begin{bmatrix} -\sin\theta_e \\ \cos\theta_e \end{bmatrix}. \tag{7}$$

III. The Design of MLESO for PMLSM

In general, the most of transfer function of disturbance observers is similar to a first or second-order low pass filter[19], so the high-frequency noise is easy to be removed.

Taking linear extended state observer (LESO) as an example, it cannot avoid the influence of signals with a frequency lower than the cutoff frequency. However, the DC bias and drift of phase current are inevitable in practice, because the measurement sensors are sensitive to the temperature. These measurement errors maybe reduce the reliability and precision of sensorless control. Hence, a modified LESO will be proposed to improve the control performance.

Firstly, the back EMF can be regarded as a disturbance, which can be written as in frequency domain:

$$\begin{bmatrix} e_\alpha \\ e_\beta \end{bmatrix} = \begin{bmatrix} u_\alpha \\ u_\beta \end{bmatrix} - (Ls + R_s)\begin{bmatrix} i_\alpha \\ i_\beta \end{bmatrix}, \tag{8}$$

Where e_d and e_q are back EMF in the *dq* synchronous reference frame, $L=L_d=L_q$ due to they are almost equal and not sensitive to current variation. The system (8) can be written as

$$\begin{bmatrix} \dot{i}_\alpha \\ \dot{i}_\beta \end{bmatrix} = \frac{1}{L}\begin{bmatrix} u_\alpha \\ u_\beta \end{bmatrix} - \frac{R_s}{L}\begin{bmatrix} i_\alpha \\ i_\beta \end{bmatrix} + \begin{bmatrix} e_\alpha \\ e_\beta \end{bmatrix}. \tag{9}$$

The design method of α-axis and β-axis is the same, take α-axis as an example. In α-axis, letting $x_1=i_\alpha$, $u=u_\alpha$, $f_\alpha=-i_\alpha R_s/L+e_\alpha+d$, d is unmodeled dynamics. The system (9) can be rewritten as a universal one-order state space model:

$$\dot{x}_1(t) = bu(t) + f_\alpha(t). \tag{10}$$

Where $b=1/L$, $f_\alpha(t)$ represents the total disturbance, which contains the information of back EMF. Letting an extended state $x_2(t)=f_\alpha(t)$, the extended state system can be obtained:

$$\begin{cases} \dot{x}_1(t) = bu(t) + x_2, \\ \dot{x}_2(t) = \dot{f}_\alpha(t). \end{cases} \tag{11}$$

Hence, the LESO can be written as:

$$\begin{cases} e = z_1 - x_1, \beta_1=2\omega, \quad \beta_2=\omega^2, \\ \dot{z}_1 = z_2 - \beta_1 e + bu, \\ \dot{z}_2 = -\beta_2 e. \end{cases} \tag{12}$$

Denote ω as the observer bandwidth. The z_1 and z_2 will track x_1 and f respectively with appropriate ω. The transfer function of LESO can be given as [20]:

$$\begin{cases} G_{LESO1}(s) = \dfrac{z_1(s)}{x_1(s)} = \dfrac{\beta_1 s + \beta_2}{s^2 + \beta_1 s + \beta_2}, \\ G_{LESO2}(s) = \dfrac{z_2(s)}{x_1(s)} = \dfrac{\beta_2 s}{s^2 + \beta_1 s + \beta_2}. \end{cases} \tag{13}$$

The observer gains can be selected by bandwidth-parameterization method[21], such that all the observer eigenvalues are placed at $-\omega_o$, then $\beta_1=2\omega_o$, $\beta_2=\omega_o^2$.

The frequency response of LESO is shown in Fig.2. It is clear that conventional LESO with the LPF characteristics only removes the high-frequency noise. Therefore, an MLESO with bandpass characteristics is proposed as follows:

$$\begin{cases} G_{MLESO1}(s) = \dfrac{2\omega s + \omega^2}{s^2 + 2\omega s + \omega^2} - \dfrac{2\omega' s + \omega'^2}{s^2 + 2\omega' s + \omega'^2}, \\ G_{MLESO2}(s) = \dfrac{\omega^2 s}{s^2 + 2\omega s + \omega^2} - \dfrac{\omega'^2 s}{s^2 + 2\omega' s + \omega'^2}. \end{cases} \tag{14}$$

Where ω' should be smaller than ω, they are set to be satisfied that $\omega > \omega' \geq 0$. When set $\omega=500$ and $\omega'=5$, the frequency response of MLESO is shown in Fig.2.

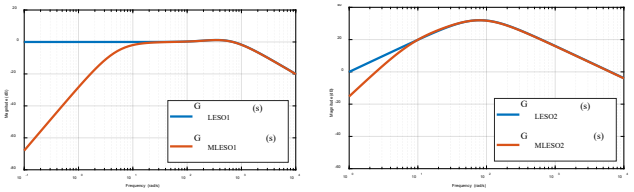

(a) $G_{LESO1}(s)$ and $G_{MLESO1}(s)$. (b) $G_{LESO2}(s)$ and $G_{MLESO2}(s)$.

Fig. 2. Frequency response comparison of LESO and MLESO: (a) $G_{LESO1}(s)$ and $G_{MLESO1}(s)$, (b) $G_{LESO2}(s)$ and $G_{MLESO2}(s)$.

In order to compare the two observers, the observer bandwidth is the same ($\omega=500$) in both. Obviously, the proposed MLESO, the same as the LESO, has robustness in the high-frequency region. The different performances reflect different influences on the low-frequency region caused by the modified LESO. MLESO demonstrates effective attenuation on low-frequency components of measured voltage and current, such as DC bias, a drift of current, and so forth.

The structure diagram of MLESO is shown in Fig.3, and the structure of estimation block and PLL are given in Fig.4 and Fig.5 respectively.

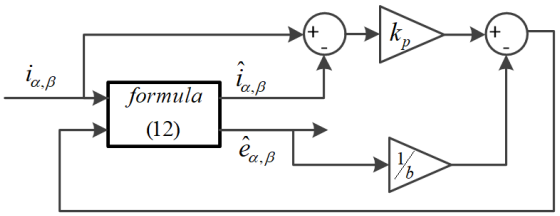

Fig. 3. The structure diagram of MLESO

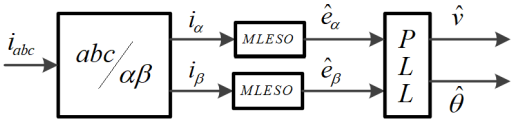

Fig. 4. Block diagram of estimation

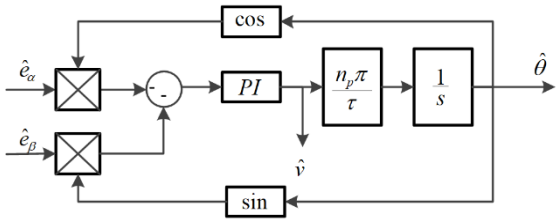

Fig. 5. Block diagram of PLL

IV. The Control System of PMLSM

In this part, a control scheme based on linear active rejection disturbance control (LADRC) and feedforward control (FFC) is introduced to improve the disturbance rejection and response speed of the PMLSM. The control system of PMLSM is given in Fig.6.

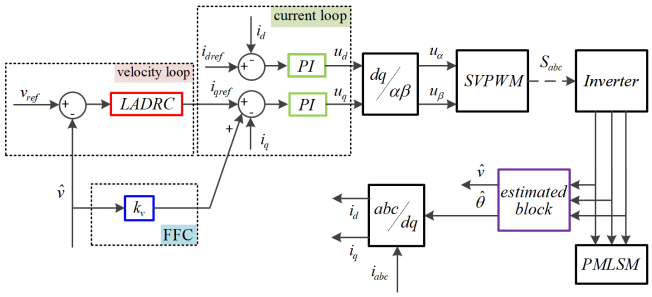

Fig. 6. Control system of PMLSM

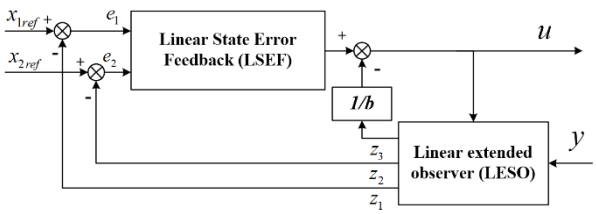

Fig. 7. Structure diagram of LADRC

A. The structure of LADRC

A two-order LADRC controller can be designed in Fig.7. LADRC consists of the linear extended state observer (LESO) and the linear state error feedback law (LSEF). LESO is responsible for accurately estimate the total disturbance. The LSEF is responsible for the realization of the desired signal by using a feedback controller, such as linear proportional differential control. Hence, the effect of LADRC largely depends on the estimation accuracy of the total disturbance. In this part, the second-order LADRC controller is selected.

Based on a general second-order state space model (15), a third-order extended state system (16) can be obtained, where $y(t)$ is the speed of the linear motor, which is defined as the first state $x_1(t)$ as usual; the second state $x_2(t)$ is derivative of $x_1(t)$, $f(t)$ represents the total disturbance, which including unmodeled dynamics and variation of the parameters.

$$\begin{cases} \dot{x}_1(t) = x_2(t), \\ \dot{x}_2(t) = bu(t) + f(t), \\ y(t) = x_1(t). \end{cases} \tag{15}$$

$$\begin{cases} \dot{x}_1(t) = x_2(t), \\ \dot{x}_2(t) = x_3(t) + bu(t), \\ \dot{x}_3(t) = f(t), \\ y(t) = x_1(t). \end{cases} \tag{16}$$

Hence, the LESO can be written as:

$$\begin{cases} e = z_1 - x_1, \\ \dot{z}_1(t) = z_2(t) - \beta_1 e(t), \\ \dot{z}_2(t) = z_3(t) - \beta_2 e(t) + bu(t), \\ \dot{z}_3(t) = -\beta_3 e(t). \end{cases} \tag{17}$$

The parameter selection method is the same as in section III, so $\beta_1=3\omega_o$, $\beta_2=3\omega_o^2$, $\beta_3=\omega_o^3$. After Laplace transform, equation (17) can be rewritten as (18).

$$\begin{cases} z_1(s) = \dfrac{\beta_1 s^2 + \beta_2 s + \beta_3}{s^3 + \beta_1 s^2 + \beta_2 s + \beta_3} y(s) + \dfrac{b_0 s}{s^3 + \beta_1 s^2 + \beta_2 s + \beta_3} u(s) \\ z_2(s) = \dfrac{\beta_2 s^2 + \beta_3 s}{s^3 + \beta_1 s^2 + \beta_2 s + \beta_3} y(s) + \dfrac{b_0 s^2 + b_0 \beta_1 s}{s^3 + \beta_1 s^2 + \beta_2 s + \beta_3} u(s) \\ z_3(s) = \dfrac{\beta_3 s^2}{s^3 + \beta_1 s^2 + \beta_2 s + \beta_3} y(s) - \dfrac{b_0 \beta_3}{s^3 + \beta_1 s^2 + \beta_2 s + \beta_3} u(s) \end{cases} \tag{18}$$

Base on the estimation of the state of the system, the linear PD controller is used to track the reference value $x_{1ref}=v_{ref}$ and the estimation of the total disturbance is subtracted from PD control law to compensate the disturbance. Hence, in the s domain the transfer function of the LSEF can be expressed as:

$$\begin{cases} u(s) = \dfrac{u_0(s) - z_3(s)}{b}, \\ u_0(s) = k_p \left[x_{1ref}(s) - z_1(s) \right] - k_d z_2(s). \end{cases} \tag{19}$$

The parameters k_p and k_d can also be selected by bandwidth-parameterization method, generally $k_p=2\omega_c$, $k_d=\omega_c^2$. Denote ω_c as the observer bandwidth. Formula (20) can be obtained by taking formula (19) into formula (15),

$$\dot{x}_2(s) = u_0(s) - z_3(s) + f(s). \tag{20}$$

Obviously, when z_3 equals $f(s)$, the total interference will be eliminated.

The transfer function of LADRC can be obtained by combining formula (18) and (19), as shown in (21).

$$u(s) = G_{uy}(s) G_{ur}(s) ref(s) - G_{uy}(s) y(s), \tag{21}$$

Where,

$$G_{ur}(s) = \frac{k_p s^3 + k_p \beta_1 s^2 + k_p \beta_2 s + k_p \beta_3}{\left(k_p \beta_1 + k_d \beta_2 + \beta_3\right) s^2 + \left(k_p \beta_2 + k_d \beta_3\right) s + k_p \beta_3}, \tag{22}$$

$$G_{uy}(s) = \frac{1}{b_0} \cdot \frac{\left(k_p \beta_1 + k_d \beta_2 + \beta_3\right) s^2 + \left(k_p \beta_2 + k_d \beta_3\right) s + k_p \beta_3}{s^3 + (\beta_1 + k_d) s^2 + (\beta_1 k_d + \beta_2 + k_p) s}. \tag{23}$$

B. Stability analysis

In this section, the stability of the whole system is proved. The transfer function block diagram of the feedback path of PMLSM system is shown in Fig.8.

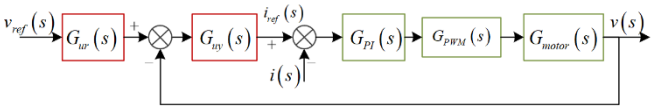

Fig. 8. Transfer function block diagram of feedback path

Among them, $G_{PI}(s)$ is the transfer function of PI controller in the current loop, $G_{PWM}(s)$ is the equivalent transfer function of the SVPWM, and the $G_{motor}(s)$ is the approximate model of PMLSM in frequency domain. The Bode diagram of the PMLSM system is shown in Fig.9, at 5.28×10^6 rad/s the phase margin is greater than zero, which is proved that the control system is stable.

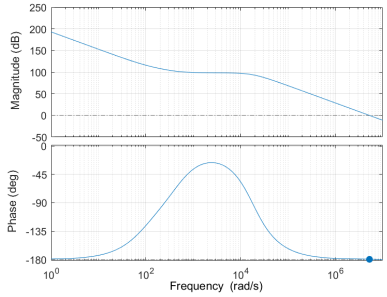

Fig. 9. The Bode diagram of PMLSM system

C. FFC

In order to improve the dynamic performance of tracking, the FFC based on speed signal is introduced into the control system. By adjusting the coefficients k_v to compensate partially to improve the system response speed.

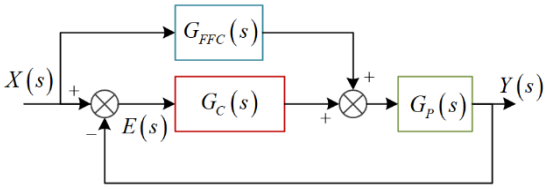

Fig. 10. The equivalent transfer function block diagram of simplified system

The equivalent transfer function of the system is shown in Fig.10, it can be obtained as

$$G(s) = \frac{Y(s)}{X(s)} = \frac{G_P(s)G_C(s) + G_{FFC}(s)G_P(s)}{G_P(s)G_C(s) + 1}. \tag{24}$$

It is clear when $G_{FFC}(s)=1/G_P(s)$, $G(s)=1$, so $X(s)=Y(s)$ and $E(s)=0$. In addition, the path of feedforward controller is the feedforward path is independent of the feedback path, and the eigenvalues of the system remain unchanged, so the system is still stable.

V. Simulated Results

In order to verify the performance of proposed control strategy based on the modified linear error state observer, a MATLAB/Simulink model based PMLSM sensorless control system is built, which is shown in Fig.11. The parameters of PMLSM are shown in the Table I.

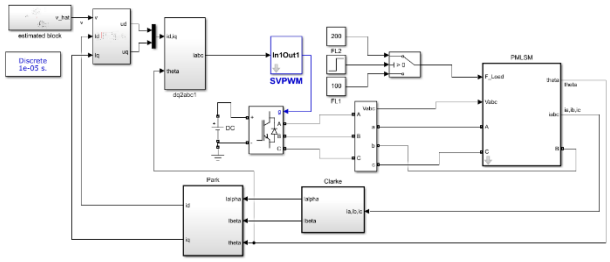

Fig. 11. The diagram of simulink model

TABLE I. PARAMETERS OF PMLSM

PARAMETERS OF PMLSM		
Denotation	***Symbol***	***Value***
Flux linkage (*Wb*)	λ_{PM}	***0.55***
Stator inductance (*mH*)	***L***	***3.45***
Stator resistance (Ω)	R_s	***1.23***
Number of pole pairs	n_p	***2***
Pole pitch (*cm*)	τ	***3***
Frictional coefficient (*N·s/m*)	***D***	***2***
Primary weight (*kg*)	$M=m+m_0$	***32***

The parameters of MLESO are set to $\omega=500$ and $\omega'=5$ in α and β axis.

At zero speed, the back EMF is zero, so the proposed method can't get the mover position before starting the linear motor, and the back EMF value is very small when the motor is running at a low speed, so the signal sampling is easy to be disturbed. Therefore, only when the motor is accelerated to a certain speed by using the speed open-loop method can the estimated mover position and speed information be used for speed closed-loop control.

In simulation, v_{ref} is changed from 1 m/s to 1.4 m/s at 0.2s, and, finally, set to 1.8m/s at 0.4s. In Fig.12, it is clear that the actual velocity can reach to the reference value within 0.015s, and the estimated velocity can track the actual speed closely. It illustrates that a good estimated performance in steady state and transient state. As shown in Fig.13, the back EMF of α and β axis can be obtained, its amplitude varies with the speed.

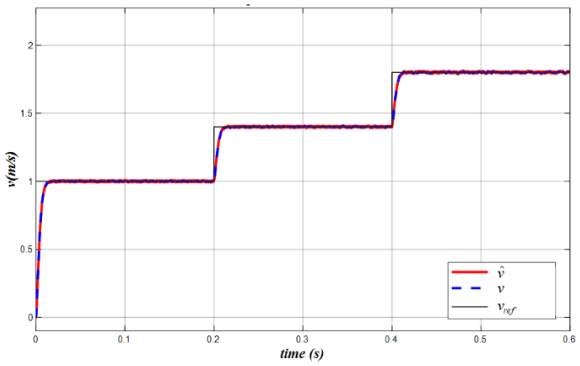

Fig. 12. The estimated velocity

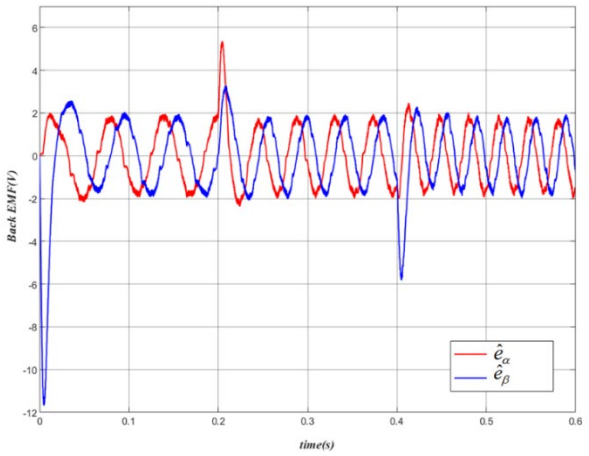

Fig. 13. The back EMF in α and β axis

In order to verify the performance and disturbance rejection ability of the proposed method are better than conventional control, a LADRC and a PI controller are applied in the velocity loop respectively, the parameters of LADRC are $\omega_c=500$, $\omega_o=20\omega c$, and $b=1/L$, the parameters of PI controller in α and β axis both are $k_{pv}=20$, $k_{iv}=8000$. In order to ensure fairness, PI control is used in the current loop in these two control structures. Its parameters are set as $k_{pc}= 53$, $k_{ic}= 5200$. In this simulation, the load force is changed from 100N to 200N at 0.3s. The speed response curve is shown in Fig.14. The proposed control can ensure the smooth speed transition and no overshoot when the speed reference value changes suddenly at 0.2s and 0.4s, and the steady-state accuracy of speed is also improved. In addition, velocity also can be maintained while the load step to 200N at 0.3s due to its strong disturbance rejection ability. However, in order to achieve a faster response speed, the PI controller has a larger overshoot.

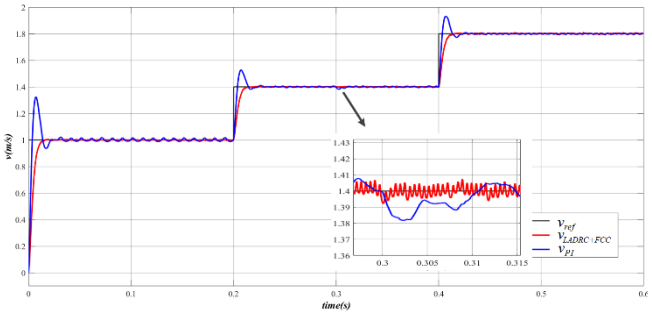

Fig. 14. Comparison of speed response of PI and proposed method

However, in order to achieve a faster response speed, the PI controller has a larger overshoot. In order to further improve the dynamic performance, FFC is added. The speed response before and after FFC addition is shown in Fig.15. It can be clearly seen that the response speed is faster and the transient effect is better after adding feedforward.

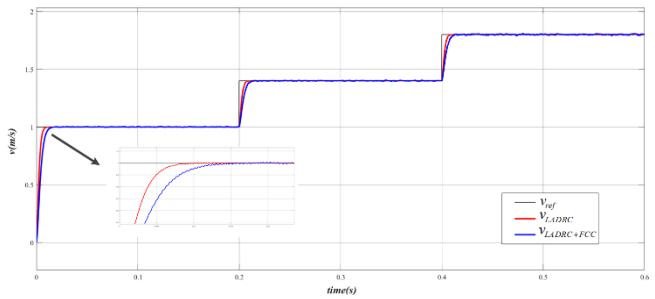

Fig. 15. Comparison of speed response with and without FFC

VI. Conclusion

The proposed control strategy is based on MLESO with band-pass filter characteristics, so that the low-frequency measurement error and DC offset are removed. LADRC controller is introduced into the velocity loop to enhance the disturbance rejection performance of the system and keep the speed stable when the speed reference value and load change suddenly. Finally, FFC is added to further optimize the transient performance and improve the response speed.

VII. Acknowledge

This paper is supported by China Scholarship Council.

VIII. References

[1] W. Zhao, S. Jiao, Q. Chen, D. Xu and J. Ji, "Sensorless Control of a Linear Permanent-Magnet Motor Based on an Improved Disturbance Observer," in IEEE Transactions on Industrial Electronics, vol. 65, no. 12, pp. 9291-9300, Dec. 2018, doi: 10.1109/TIE.2018.2823660.

[2] D. Jiang, W. Yu, J. Wang, Y. Zhao, Y. Li and Y. Lu, "A Speed Disturbance Control Method Based on Sliding Mode Control of Permanent Magnet Synchronous Linear Motor," in IEEE Access, vol. 7, pp. 82424-82433, 2019, doi: 10.1109/ACCESS.2019.2922765.

[3] H. Lu; Y. Xu. Speed and position estimation algorithm of permanent magnet linear synchronous motor based on augmented extended Kalman filter, Proceedings of the CSEE, Vol.29, No.33, 90-94, 2009.

[4] D. Casadei, F. Profumo, G. Serra and A. Tani, "FOC and DTC: two viable schemes for induction motors torque control," in IEEE Transactions on Power Electronics, vol. 17, no. 5, pp. 779-787.

[5] J. Shi, T. Liu, and Y. Chang, “Position control of an interior permanent-magnet synchronous motor without using a shaft position sensor,” IEEE Trans. Ind. Electron., vol. 54, no. 4, pp. 1989-2000, Jun. 2007.

[6] S. Morimoto, K. Kawamoto, M. Sanada, and Y. Takeda, “Sensorless control strategy for salient-pole PMSM based on extended EMF in rotating reference frame,” IEEE Trans. Ind. Appl., vol. 38, no. 4, pp. 1054-1061, Jul/Aug. 2002.

[7] A. V. S. Krishna and S. Kumar, "Position-sensorless operation of brushless permanent-magnet machines — A review," 2014 International Conference on Green Computing Communication and Electrical Engineering (ICGCCEE), 2014, pp. 1-10.

[8] Yen-Shin Lai, Fu-Shan Shyu and Wei-Hwa Rao, "Novel back-EMF detection technique of brushless DC motor drives for whole duty-ratio range control," 30th Annual Conference of IEEE Industrial Electronics Society, 2004. IECON 2004, 2004, pp. 2729-2732.

[9] P. Damodharan and K. Vasudevan, "Sensorless Brushless DC Motor Drive Based on the Zero-Crossing Detection of Back Electromotive Force (EMF) From the Line Voltage Difference," in IEEE Transactions on Energy Conversion, vol. 25, no. 3, pp. 661-668.

[10] M. J. Corley and R. D. Lorenz, "Rotor position and velocity estimation for a salient-pole permanent magnet synchronous machine at standstill and high speeds," in IEEE Transactions on Industry Applications, vol. 34, no. 4, pp. 784-789.

[11] Hyunbae Kim, M. C. Harke and R. D. Lorenz, "Sensorless control of interior permanent-magnet machine drives with zero-phase lag position estimation," in IEEE Transactions on Industry Applications, vol. 39, no. 6, pp. 1726-1733.

[12] A. N. Smith, S. M. Gadoue and J. W. Finch, "Improved Rotor Flux Estimation at Low Speeds for Torque MRAS-Based Sensorless Induction Motor Drives," in IEEE Transactions on Energy Conversion, vol. 31, no. 1, pp. 270-282.

[13] F. Genduso, R. Miceli, C. Rando and G. R. Galluzzo, "Back EMF Sensorless-Control Algorithm for High-Dynamic Performance PMSM," in IEEE Transactions on Industrial Electronics, vol. 57, no. 6, pp. 2092-2100.

[14] D. Tran and Y. K. Tan, "Sensorless Illumination Control of a Networked LED-Lighting System Using Feedforward Neural Network," in IEEE Transactions on Industrial Electronics, vol. 61, no. 4, pp. 2113-2121.

[15] J. Kim, S. Choi, K. Cho and K. Nam, "Position Estimation Using Linear Hall Sensors for Permanent Magnet Linear Motor Systems," in IEEE Transactions on Industrial Electronics, vol. 63, no. 12, pp. 7644-7652, Dec. 2016.

[16] M. A. M. Cheema, J. E. Fletcher, M. Farshadnia, D. Xiao and M. F. Rahman, "Combined Speed and Direct Thrust Force Control of Linear Permanent-Magnet Synchronous Motors With Sensorless Speed Estimation Using a Sliding-Mode Control With Integral Action," in IEEE Transactions on Industrial Electronics, vol. 64, no. 5, pp. 3489-3501.

[17] B. Du, S. Wu, S. Han and S. Cui, "Application of Linear Active Disturbance Rejection Controller for Sensorless Control of Internal Permanent-Magnet Synchronous Motor," in IEEE Transactions on Industrial Electronics, vol. 63, no. 5, pp. 3019-3027.

[18] R. Leidhold and P. Mutschler, "Speed sensorless control of a long-stator linear synchronous-motor arranged by multiple sections," 31st Annual Conference of IEEE Industrial Electronics Society, 2005. IECON 2005., 2005, pp. 6.

[19] A. Apte, V. A. Joshi, H. Mehta and R. Walambe, "Disturbance-Observer-Based Sensorless Control of PMSM Using Integral State Feedback Controller," in IEEE Transactions on Power Electronics, vol. 35, no. 6, pp. 6082-6090.

[20] H. Li, Y. Qu, J. Lu and S. Li, "A Composite Strategy for Harmonic Compensation in Standalone Inverter Based on Linear Active Disturbance Rejection Control, " in Energies 2019, 12, 2618.

[21] Gao, Z. Scaling and Parameterization Based Controller Tuning. American Control Conference, 2003.